OPEN ACCESS
The American Journal of Chinese Medicine, Vol. 49, No. 6, 1449–1471

DOI: 10.1142/S0192415X21500683



# The Role of Ophiopogonin D in Atherosclerosis: Impact on Lipid Metabolism and Gut Microbiota

Ya-Xin Zhang,*[,a] Shan-Shan Qu,*[,a] Li-Hua Zhang,[§,a] Yu-Yan Gu,* Yi-Hao Chen,*
Zhi-Yong Huang,[¶] Meng-Hua Liu,[†] Wei Zou,** Jing Jiang,* Jun-Qi Chen,[‖]
Yu-Jue Wang[‡] and Feng-Hua Zhou*[,††]

*School of Traditional Chinese Medicine
[†]School of Pharmaceutical Sciences
[‡]Department of Laboratory Animal Administration Center
Southern Medical University
Guangzhou 510515, P. R. China
[§]Department of Gynaecology, Integrated Hospital of Traditional Chinese Medicine
Southern Medical University
Guangzhou 510310, P. R. China
[¶]Department of Otolaryngology
[‖]Department of Rehabilitation Medicine
The Third Affiliated Hospital, Southern Medical University
Guangzhou 510630, P. R. China
**NHC Key Laboratory of Birth Defects Research
Prevention and Treatment Hunan Provincial Maternal
and Child Health Care Hospital
Changsha 410008, P. R. China
[††]The Fifth Affiliated Hospital, Southern Medical University
Guangzhou 510920, P. R. China

Published 14 July 2021

Correspondence to: Prof. Feng-Hua Zhou, Dr. Jun-Qi Chen and Dr. Yu-Jue Wang, The Fifth Affiliated Hospital, Southern Medical University, No. 566 Congcheng Avenue, Conghua District, Guangzhou, P. R. China; School of Traditional Chinese Medicine, Southern Medical University, No. 1023, South Shatai Road, Guangzhou, P. R. China. Tel: (+86) 20-6164-8767, E-mail: Wendyzhou515@126.com (F.-H. Zhou); Department of Rehabilitation Medicine, The Third Affiliated Hospital of Southern Medical University, No. 183, West Zhongshan Avenue, Guangzhou, P. R. China. Tel: (+86) 20-6278-4240, E-mail: meixibao@126.com (J.-Q. Chen); Department of Laboratory Animal Administration Center, Southern Medical University, No.1023, South Shatai Road, Guangzhou, P. R. China. Tel: (+86) 20-6164-8424, E-mail: yujue.wang@qq.com (Y.-J. Wang)
[a]These authors contributed equally to this work.

Abstract: Gut microbiota has been proven to play an important role in many metabolic diseases and cardiovascular disease, particularly atherosclerosis. Ophiopogonin D (OPD), one of the effective compounds in *Ophiopogon japonicus*, is considered beneficial to metabolic syndrome and cardiovascular diseases. In this study, we have illuminated the effect of OPD in ApoE knockout (ApoE$^{-/-}$) mice on the development of atherosclerosis and gut microbiota. To investigate the potential ability of OPD to alleviate atherosclerosis, 24 eight-week-old male ApoE$^{-/-}$ mice (C57BL/6 background) were fed a high-fat diet (HFD) for 12 weeks, and 8 male C57BL/6 mice were fed a normal diet, serving as the control group. ApoE$^{-/-}$ mice were randomly divided into the model group, OPD group, and simvastatin group ($n = 8$). After treatment for 12 consecutive weeks, the results showed that OPD treatment significantly decreased the plaque formation and levels of serum lipid compared with those in the model group. In addition, OPD improved oral glucose tolerance and insulin resistance as well as reducing hepatocyte steatosis. Further analysis revealed that OPD might attenuate atherosclerosis through inhibiting mTOR phosphorylation and the consequent lipid metabolism signaling pathways mediated by SREBP1 and SCD1 *in vivo* and *in vitro*. Furthermore, OPD treatment led to significant structural changes in gut microbiota and fecal metabolites in HFD-fed mice and reduced the relative abundance of *Erysipelotrichaceae* genera associated with cholesterol metabolism. Collectively, these findings illustrate that OPD could significantly protect against atherosclerosis, which might be associated with the moderation of lipid metabolism and alterations in gut microbiota composition and fecal metabolites.

*Keywords*: Atherosclerosis; Ophiopogonin D; Gut Microbiota; Lipid Metabolism; Metabolites.



## Introduction

Cardiovascular diseases (CVDs) endanger human health and continue to be a leading cause of death worldwide (Lacy *et al.*, 2019). Atherosclerosis, the common pathological basis of most CVDs, is characterized by the formation of atherosclerotic lesions within the arterial wall (Yu *et al.*, 2019). The etiology of atherosclerosis is complex, including several possible risk factors such as dyslipidemia, hypertension, type 2 diabetes, and hyperglycaemia (Paoletti *et al.*, 2006; Martin-Timon *et al.*, 2014). Atherosclerosis is initiated as lipid particles accumulate by subsequently trapping in vessel walls. Decreasing cholesterol accumulation is an effective way to alleviate atherosclerosis injury. Increased levels of blood lipid markers, such as triglycerides, low-density lipoprotein cholesterol, total cholesterol, are the main risk factors for the occurrence and development of atherosclerosis. Although a variety of statins are used as first-line pharmacotherapy for controlling blood lipid levels in clinical practice, their side effects, such as statin-induced renal disease, muscle damage and liver injury, cannot be ignored (Simic and Reiner, 2015). Therefore, there is a pressing need for an economical and effective method to improve the treatment of atherosclerosis.

In past decades, various studies have demonstrated that the gut microbiome plays an important role in metabolic syndrome, especially CVDs (Jonsson and Backhed, 2017). The gut microbiota regulates many metabolic processes of the host, including energy homeostasis, glucose metabolism, and lipid metabolism (Sonnenburg and Backhed, 2016).

Indeed, the gut microbiome acts as an endocrine organ, generating bio-active metabolites such as short-chain fatty acids (SCFAs), secondary bile acids and trimethylamine N-oxide (TMAO), which can impact host physiology (Tang *et al.*, 2017; Ohira *et al.*, 2017). In particular, TMAO has been shown to be a predictor of incident CVD events (Park *et al.*, 2019). These findings suggest that the gut microbiome may be a potential target for decreasing the accumulation of plasma-derived lipids, exerting beneficial effects on atherosclerosis.

Ophiopogonin D (OPD) is a main pharmacological compound of *Ophiopogon japonicus*, which is a traditional Chinese medicine widely used for thousands of years. Recent studies show that OPD suppresses inflammation and inhibits oxidant stress, thereby exerting anticancer activity (Huang *et al.*, 2015, 2017; Lee *et al.*, 2018). Additionally, OPD has been demonstrated to be effective in treating CVDs. OPD alleviates cardiac hypertrophy through inhibiting the expression of NF-κB by up-regulating CYP2J3 to suppress inflammation (Wang *et al.*, 2018), improves metabolic syndrome induced by a HFD, and changes the gut microbiota (Chen *et al.*, 2018). Since gut microbiota has an important impact on the development of atherosclerosis, regulation of gut microbiota disorder by OPD might be a new target for the prevention of atherosclerosis. However, the underlying mechanism of OPD in atherosclerosis is still unknown.

This study aimed to examine the efficacy of OPD in the prevention of atherosclerosis, which has not been investigated previously. Here, apolipoprotein E knockout ($ApoE^{-/-}$) mice were fed a HFD to replicate the atherosclerosis model. Both the area of the atherosclerotic lesion and the levels of serum lipids were measured. The gut microbiota of the mice was identified by 16S rDNA sequencing, and the fecal metabolites were investigated by $^{1}H$ NMR spectroscopy. Additionally, we also determined the involvement of pathways related to lipid metabolism *in vivo* and *in vitro* using RT-qPCR and western blotting to explore the potential mechanism.

## Materials and Methods

### *Animals and Treatments*

24 eight-week-old $ApoE^{-/-}$ male mice (from the C57BL/6 background) and 8 C57BL/6 male mice were purchased from Beijing Vital River Laboratory Animal Technology Co., Ltd. (Beijing, China) and housed in the Animal Laboratory Centre of Southern Medical University. It was a specific pathogen-free environment with 22°C room temperature, 55 ± 5% relative humidity, a 12 h light/dark cycle, and freely available food and water. In this study, the $ApoE^{-/-}$ mice were on a HFD containing 21% fat and 0.15% cholesterol (Guangdong Medical Laboratory Animal Centre, Guangdong, China) for 12 weeks. C57BL/6 mice in the control group were fed a normal-chow diet. $ApoE^{-/-}$ mice were randomly divided into three groups ($n$ = 8): the model group, OPD group (98% purity; 0.5 mg/kg/d) and simvastatin group (5 mg/kg/d). The corresponding drugs were administered by oral gavage once daily for 12 consecutive weeks, and 0.9% sterile saline was administered by oral gavage once a day to the mice in model and control group. Animals were sacrificed after 12 weeks of treatment. Fasting blood, liver tissues, heart,

and aortic tissues were collected. All animal experimental procedures were conducted in accordance with international guidelines and were approved by Southern Medical University Animal Investigation Ethics Committee.

*Measurement of Serum Profiles*

After the 24-week experimental period, all mice were anesthetized, and cardiac puncture was performed to collect blood samples. The serum was separated by centrifuging at 3000 rpm/min for 15 min and then subjected to analysis of lipid concentrations, including low-density lipoprotein cholesterol (LDL-C), total cholesterol (TC), triglycerides (TG), and high-density lipoprotein cholesterol (HDL-C) using the corresponding assess kits. In addition, the alanine transaminase (ALT), aspartate transaminase (AST), malondialdehyde (MDA), lactate dehydrogenase (LDH), and superoxide dismutase (SOD) were determined using the corresponding assay kits (Nanjing Jiancheng Bioengineering Institute, Jiangsu, China). The level of C-Peptide was determined using an ELISA kit (Jiangsu Meimian Industry Co., Ltd., China) following the manual.

*Lesion Analysis*

The heart and aortic tissues were fixed and embedded in an optimal cutting temperature compound. Cryosections (7 μm thick) were made and stained with Oil red O (ORO) and Masson staining protocol for histopathological examination. A portion of the aorta was fixed and embedded in paraffin wax. Sections of 5 μm thickness made and stained with hematoxylin and eosin (H&E). The lipid content was quantified based on the size of aortic lesions stained with ORO, and the lesion area was calculated as a percentage of the total area of aortic root using Image J software. Three sections were examined from each sample.

*Histological Analysis of the Liver*

After collecting the blood, the livers of mice were collected and weighed. The liver was fixed in 10% paraformaldehyde and embedded in paraffin wax. Sections of 5 μm thickness were made, deparaffinized, dehydrated, then stained with H&E. A portion of the liver were fixed and embedded in optimal cutting temperature compound. Liver cryosections of 7 μm were made as per the above method and stained with ORO for histological evaluation. The liver index on a fresh weight basis was calculated according to the following formula: Liver index (%) = [weight of liver (g)/final body weight (g)] × 100 (Wang *et al.*, 2017).

*Tolerance Tests*

In the 24th week, mice were subjected to both the oral glucose tolerance test (OGTT) and the insulin tolerance test (ITT). Mice fasted for 16 h before OGTT, then weighed and administered glucose solution by oral gavage at 2.0 g/kg body weight. The blood glucose

was measured before (0 min) and at 15, 30, 60, and 120 min after glucose administration, respectively (Ardiansyah *et al.*, 2018). For ITT, the mice were fasted for 6 h, then injected intraperitoneally with insulin at 0.75 U/kg body weight (Nagy and Einwallner, 2018). We measured the blood glucose before (0 min) and at 15, 30, 60, and 120 min after insulin administration, respectively. The area under the curve (AUC) of the blood glucose concentrations during OGTT and ITT was calculated.

### *Real-Time qPCR Analysis*

The total RNA in the liver was extracted using a Takara Universal RNA Extraction Kit. The RNA samples were reverse-transcribed into cDNA using Primescript Master Mix kits, and the cDNA samples were then amplified. Real-time quantitative PCR was performed with the ChamQ Universal SYBR qPCR Master Mix. The qPCR condition was as follows: 95 °C for 10 min, followed by 40 cycles at 95 °C for 5 s and 60 °C for 30 s. The mRNA levels of mammalian targets rapamycin (mTOR), sterol regulatory element-binding protein1 (Srebp1), acetyl-CoA carboxylase (Acc1), and stearoyl-CoA desaturase-1 (Scd1) were analyzed and normalized to the level of Gapdh. The primer sequences are shown in Table 1.

### *Western Blot Analysis*

The protein samples were respectively collected by liver tissues or human LO2 cells using RIPA buffer. Then, the protein concentration was measured by BCA assay. An equal amount of protein (40 μg) was separated using 10% SDS-PAGE and transferred to the polyvinylidene difluoride membrane. The membrane was blocked in TBST with 5% BSA for 2 hrs at room temperature (RT). The membrane was then incubated with primary antibodies (1:1000) in TBST with 5% BSA overnight at 4 °C. After incubation with secondary antibody for 1.5 hrs at RT, the membrane was scanned, and the protein band was imaged using the chemiluminescence western blot detection system.

**Table 1. Primer Sequences for Quantitative Real-Time PCR Amplification**

| Name | Sequence 5′–3′ |
|---|---|
| Gapdh | F: AGGTCGGTGTGAACGGATTTG |
| | R: TGTAGACCATGTAGTTGAGGTCA |
| mTOR | F: ACCGGCACACATTTGAAGAAG |
| | R: CTCGTTGAGGATCAGCAAGG |
| Srebp1 | F: TGACCCGGCTATTCCGTGA |
| | R: CTGGGCTGAGCAATACAGTTC |
| Scd1 | F: TTCTTGCGATACACTCTGGTGC |
| | R: CGGGATTGAATGTTCTTGTCGT |
| Acc1 | F: ATGGGCGGAATGGTCTCTTTC |
| | R: TGGGGACCTTGTCTTCATCAT |

*Immunofluorescence Staining*

The frozen section of the liver was fixed with 10% paraformaldehyde for 10 min. The section was permeabilized in 0.2% Triton X-100 and blocked with 5% goat serum. After incubation with primary antibody overnight at 4 °C and secondary antibody for 2 hrs at RT, the slide was washed twice with PBS and then counterstained using DAPI. The image was obtained by fluorescence microscopy.

*Cell Culture and Model Establishment*

Human $LO_2$ cells were cultured with DMEM medium (Invitrogen, Carlsbad, CA, USA) supplied 10% fetal bovine serum (Invitrogen), 1% penicillin, and streptomycin (Invitrogen), in a humidified atmosphere of 5% $CO_2$ in 37 °C. The experiments were performed using cells at passages 3–5. OPD (Chendu Must Biotechnology Co., Ltd, China) and oleate (Sigma, St. Louis, MO, USA) were dissolved in dimethyl sulfoxide (DMSO) (Sigma, St. Louis, MO, USA). After seeding in a 6-well plate at a density of $4 \times 10^6$ cell/mL overnight, $LO_2$ cells were exposed to 300 μmol/L oleate solution for 24 hrs to induce cellular steatosis model.

*Cell Viability*

The cell viability was evaluated by CCK8 assay. Cells were seeded at a density of $3 \times 10^4$ cell/mL in 96-well plates and treated with OPD solution. After 24 hrs, CCK8 was added to each well and incubated at 37 °C for 40 min. The cell viability was measured based on the absorbance at 470 nm and calculated.

*Cell ORO Staining and Cell Triglycerides Assay*

Cells were cultured as above and treated with oleate solution and OPD (20, 40, 80 μmol/L) meantime for 24 hrs. $LO_2$ cells were washed with PBS and fixed with 4% paraformaldehyde for 15 min at room temperature, then rinsed with PBS. ORO staining images were captured with a microscope. In $LO_2$ cells triglycerides assay, after digesting the cells with pancreatin, the cells were centrifuged at 1000 rpm/min for 10 min and washed twice with PBS. Then, the cells were ultrasonic pulverized with PBS and subjected to measure the triglycerides level with a corresponding assay kit (Nanjing Jiancheng Bioengineering Institute, Jiangsu, China) according to the manual.

*Gut Microbiota Analysis*

Mice faeces were collected and stored at −80 °C. Fecal microbial DNA was extracted using a MOBIO PowerSoil DNA Isolation Kit according to the manufacturer's protocol. Microbiota analysis by 16S rDNA gene sequencing was conducted using Takara Bio Inc products. The V3-V4 region of the 16S rDNA gene was amplified using forward primer 338F

(5′-ACTCCTACGGGAGGCAGCA-3′) and reverse primer 806R (5′-GGACTACHVGGGTWTCTAAT-3′). PCR reactions were amplified by thermocycling (BioRad S1000 Thermal Cycler). Sequencing libraries were generated using the NEBNext Ultra DNA Library Prep Kit for Illumina. The library was sequenced on an IlluminaHiseq2500 platform, and 250 bp paired-end (PE) reads were generated (Guangdong Magigene Biotechnology Co. Ltd., Guangdong, China). Quality filtering of the PE raw reads was performed under specific filtering conditions. Using FLASH software (V1.2.11) to stitch each pair of PE reads, the original stitching sequence of raw tags was obtained. After filtering, effective clean tags were obtained. Operational taxonomic units (OTUs) with a 97% sequence similarity threshold were analyzed by Usearch software (V10). The processing of sequence data-including species annotation, statistics of effective OTUs, data normalization, and species community structure analysis were performed. For phylotype analysis, the $\alpha$ and $\beta$ diversity indices of the samples were calculated with QIIME (V1.9.1) and displayed with R software (V3.5) (Sang *et al.*, 2018).

### *$^1$H NMR Analysis of Fecal Samples*

Mice faeces were collected and stored at −80 °C. $^1$H-NMR spectroscopy was performed using a Bruker AV III 600 MHz spectrometer at 298 K using a noesygppr1d pulse sequence at 600.20 MHz. The $^1$H NMR free induction decay (FID) signal was imported into Chenomx NMR Suite (V8.3, Edmonton, Canada) for automatic Fourier transform, phase adjustment and baseline correction. Chemical shifts were referenced internally to TSP at $\delta = 0.0$ ppm. Spectral peaks in the range of 0.1–10.0 ppm were analyzed, with 0.04 ppm used as the segmented integration unit. The segmented integration values at 4.68–5.0 ppm (water peak), 0.59–0.65 ppm, 1.72–1.79 ppm, and 2.89–2.93 ppm (DSS peaks) were removed to prevent interference of residual water and DSS peaks. The area of all integrated values was then normalized, and a matrix of each segment and the corresponding integrated area value was obtained. The variable matrix and integrated area value were used as the source data for subsequent Partial Least Squares Discriminant Analysis (PLS-DA) through MetaboAnalyst (V4.0) (Zhang *et al.*, 2020).

### *Statistical Analysis*

The 16S rDNA analysis was performed by R software (V3.5), and other statistical analysis was performed using IBM SPSS software (V20) and the GraphPad Prism statistics (V6.0). The data were expressed as mean ± SD. The Student's *t*-test was used to compare the differences between two groups, and one-way analysis of variance (ANOVA) was used to compare more than two groups. A $P$-value $< 0.05$ was considered statistically significant.

## Results

### *Weight and Levels of Serum Biochemical Indicators in Mice*

Firstly, we examined the potential effect of OPD treatment on body weight and serum lipid levels in HFD-fed ApoE$^{-/-}$ mice. The result in Fig. 1 indicated that a HFD for 24 weeks

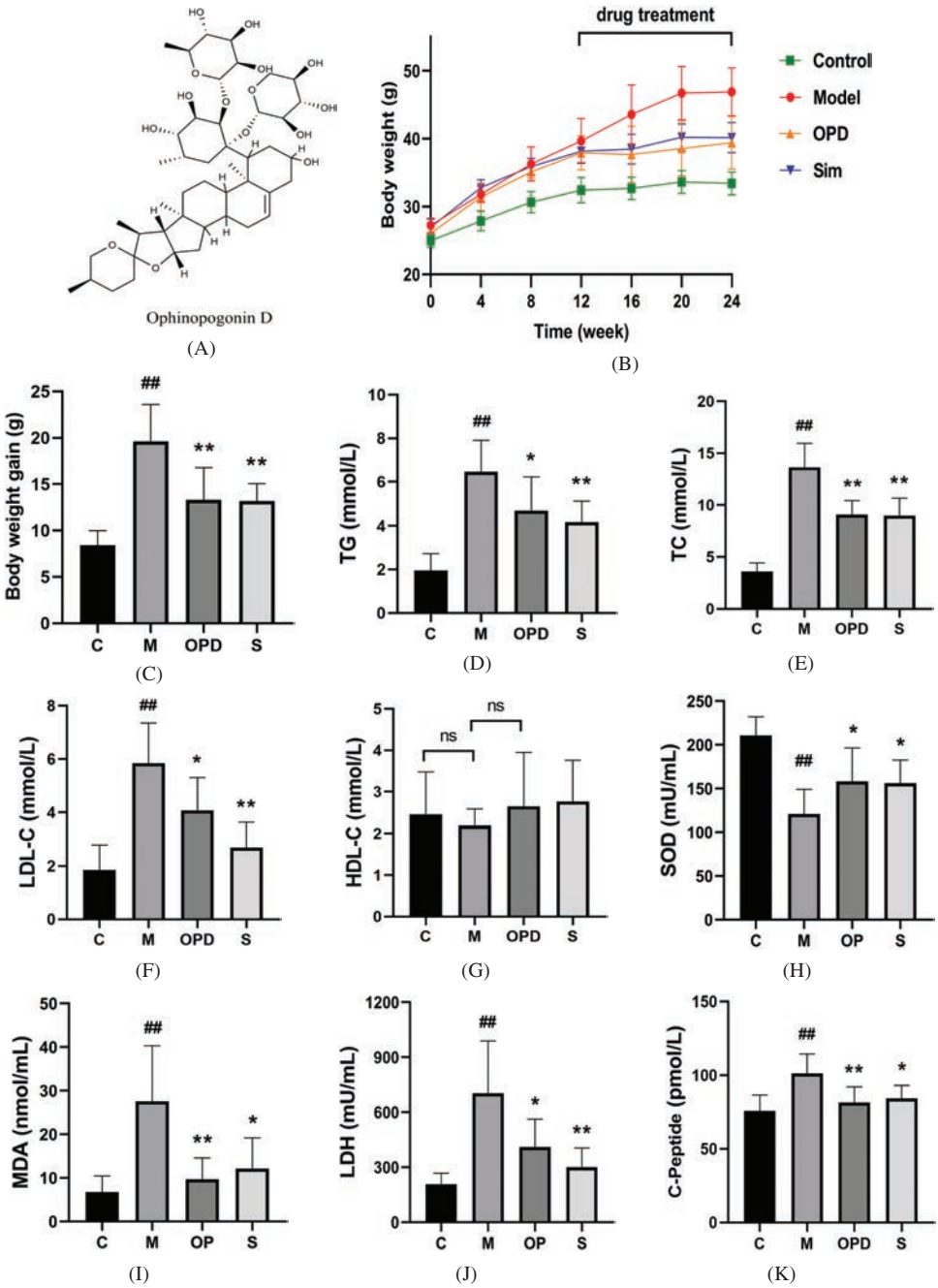


Figure 1. Ophiopogonin D prevented the increase in the body weights induced by a high-fat diet and improved the blood lipid levels and oxidant stress in ApoE$^{-/-}$ mice. (A) Ophiopogonin structure, (B) Change of body weight in the experiment period, (C) Body weight gain between the 20th f and 24th week, (D–G) The serum levels of TG, TC, LDL-C, and HDL-C, (H–K) The serum levels of SOD, MDA, LDH, and C-Peptide. Different superscript symbols indicate significant differences between groups ($^{\#}P < 0.05$ or $^{\#\#}P < 0.05$ vs. control group, $^{*}P < 0.05$ or $^{**}P < 0.01$ vs. model group).

significantly increased mice body weight. Compared with the model group, OPD significantly reduced body weight gain between the 16th and 24th weeks. In addition, there was an increase in serum levels of TG, TC, and LDL-C compared with those of the control group ($P < 0.01$). The levels of TC, TG, and LDL-C were significantly lower in OPD-treated mice than those in model mice ($P < 0.05$). The level of HDL-C was not significantly different.

It is well known that fatty acid stimulation could trigger oxidative stress reaction. The levels of MDA, LDH, and SOD were measured to evaluate the anti-oxidative effect of OPD. The results showed that the levels of MDA and LDH were increased in the model group, while SOD was decreased ($P < 0.01$) (Figs. 1H–1J). There was a marked decrease for MDA ($P < 0.01$) and LDH ($P < 0.05$) in the OPD group as well as an increase for SOD ($P < 0.05$) compared with those in the model group. C-peptide was related to increased lipid deposits and elevated smooth muscle cell proliferation in the vessel wall, contributing to atherosclerosis (Alves *et al.*, 2019). It showed that the C-peptide level in the model group was higher than that in the control group ($P < 0.05$), and OPD decreased C-peptide levels ($P < 0.05$).

### *Lesions in Mice*

To assess the effect of OPD on atherosclerotic damage, we observed the atherosclerotic lesion in the aortic sinus. As shown in Fig. 2, the HFD-fed mice developed obvious plaques in the aorta sinus. However, the percentage of the atherosclerosis lesion area in the OPD group was 0.66-fold smaller than that in the model group ($P < 0.01$). ORO staining showed that OPD treatment decreased the lipid deposition in the aortic sinus. Meanwhile, H&E staining revealed thickening of the aortic intima and thinning of the smooth muscle layer of the vascular media in the model group, while OPD ameliorated these changes. In brief, these data suggest that OPD inhibits excessive cholesterol deposition vascularly and alleviates the progression of atherosclerosis.

### *Fatty Liver Injury in Mice*

Since a HFD is one of the major reasons for the progression of liver steatosis, it was unsurprising that there was obvious liver steatosis in model group. As shown in Figs. 3A and 3B, the reduction of hepatocyte vacuolation and lipid loading in the liver in the OPD group were observed and compared with those in the model group. The liver weight and liver index of the model group were increased significantly compared to those of the control group, whereas OPD treatment significantly lowered the liver weight and liver index. HFD caused liver injury mainly through the release of ALT and AST (Lv *et al.*, 2019). Therefore, we determined the levels of ALT and AST to evaluate the effect of OPD on liver function. Compared with the control group, the activities of AST and ALT in the model group were significantly elevated ($P < 0.01$). The AST and ALT activities were significantly decreased in the OPD group compared with those of the model group ($P < 0.01$). Collectively, OPD treatment notably ameliorates macrovesicular steatosis of the liver in ApoE$^{-/-}$ mice induced by a HFD.

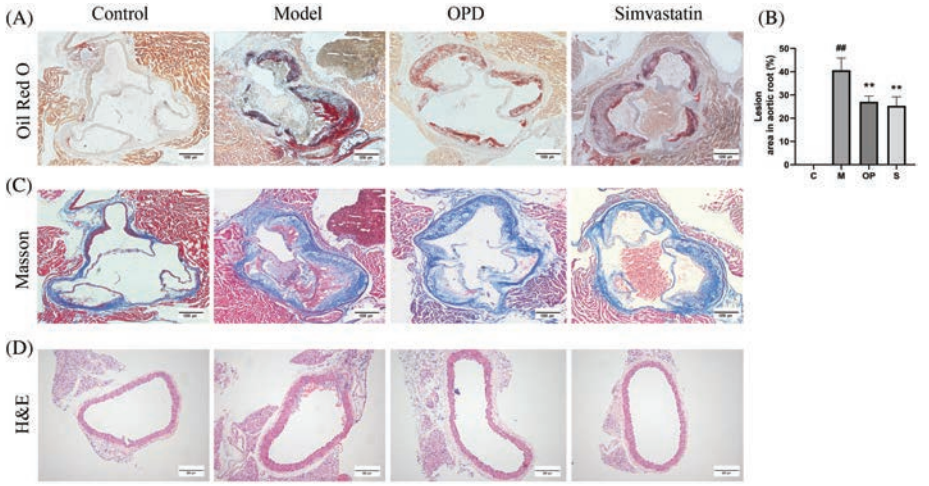


Figure 2. Ophiopogonin D alleviated the progression of atherosclerosis in ApoE$^{-/-}$ mice fed on HFD. (A) The cryosection of aortic root stained with Oil red O. (B) The cryosection of aortic root stained with Masson staining. (C) The paraffin section of the aorta stained with H&E staining. (D) The percentage of lesion area in aortic root quantified using Image J analysis software. Different superscript symbols indicate significant differences between groups ($^{\#}P < 0.05$ or $^{\#\#}P < 0.05$ vs. control group, $^{*}P < 0.05$ or $^{**}P < 0.01$ vs. model group).

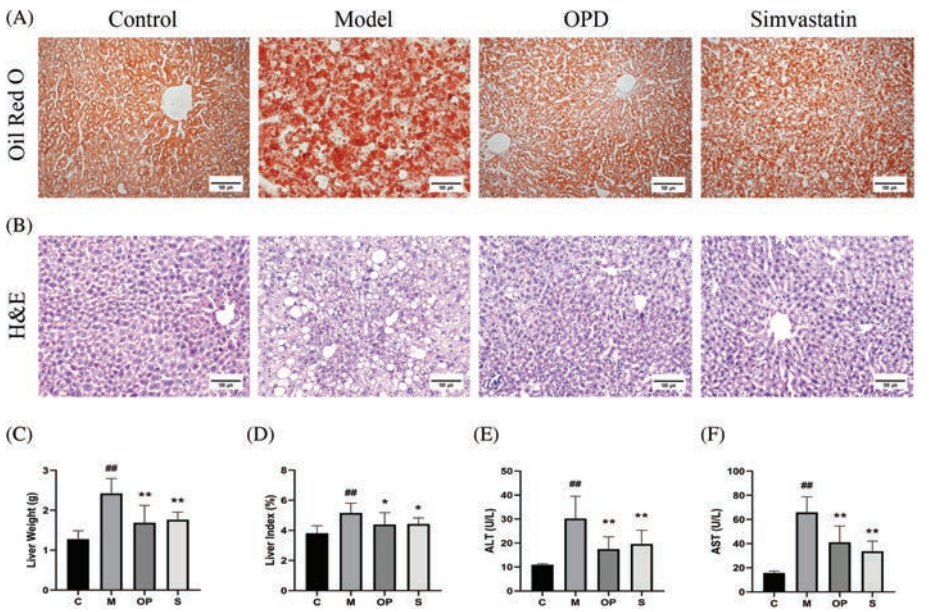


Figure 3. Ophiopogonin D inhibited HFD-induced liver steatosis in ApoE$^{-/-}$ mice. (A) The liver cryosection stained with Oil red O. (B) The liver paraffin section stained with H&E staining. (C–D) The liver weight and liver index after 24 weeks. (E–F) The serum levels of ALT and AST. Different superscript symbols indicate significant differences between groups ($^{\#}P < 0.05$ or $^{\#\#}P < 0.05$ vs. control group, $^{*}P < 0.05$ or $^{**}P < 0.01$ vs. model group).

*Tolerance Tests in Mice*

To evaluate the effect of OPD on insulin resistance, the OGTT and ITT were performed during the 24th week. According to the OGTT result, the blood glucose concentration of mice was increased at 15, 30, 60, and 120 min following the oral glucose administration. The blood glucose levels in both the model group and drug groups were significantly higher than those of control group (Fig. 4A). However, the incremental AUC calculated for the OPD treatment group was significantly smaller than that in the model group. OGTT result indicated that OPD supplement improved the level of blood glucose in mice.

For ITT experiment, it was observed that the blood glucose concentration decreased after intraperitoneal insulin administration in all groups. The blood glucose level was significantly lower in the OPD group than that in the model group at 15 and 30 min after insulin administration ($P < 0.05$). However, there was no significant difference at 60 and 120 min between these two groups. In a word, OPD improves the insulin resistance in mice.

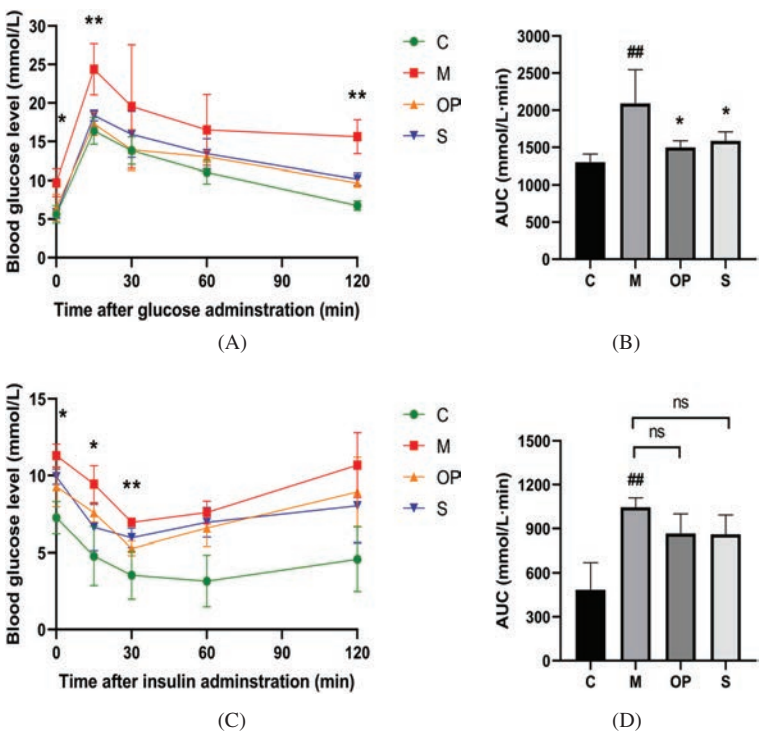


Figure 4. Ophiopogonin D improved the OGTT and ITT in ApoE$^{-/-}$ mice. (A) Blood glucose changes in the OGTT. (B) The areas under the curve (AUC) in the OGTT. (C) Blood glucose changes in the ITT. (D) The areas under the curve in the ITT. Different superscript symbols indicate significant differences between groups ($^{\#}P < 0.05$ or $^{\#\#}P < 0.05$ vs. control group, $^{*}P < 0.05$ or $^{**}P < 0.01$ vs. model group).

*Expression of mRNA and Protein in Mice Liver Tissue*

To further explore the underlying mechanism of OPD on lipid metabolism, the lipid metabolism-related gene and protein levels were examined by qPCR and western blotting. Firstly, the HFD feeding markedly upregulated the mRNA of these genes in the model group compared to those in the control group (*mTOR*, 1.49-fold; *Srebp1*, 1.92-fold; *Acc*, 1.84-fold; *Scd1*, 1.93-fold; $P < 0.05$). There was a decrease in the mRNA levels of *mTOR*, *Srebp1*, *Acc,* and *Scd1* in the OPD group compared with those of the model group (*mTOR*, 0.65-fold; *Srebp1*, 0.57-fold; *Acc*, 0.54-fold; *Scd1*, 0.5-fold; $P < 0.05$).

To evaluate the level of mTOR activation in the liver, the phosphorylation-mTOR (p-mTOR) and total mTOR expression were examined. As shown in Fig. 5E, the level of mTOR and p-mTOR (Ser2448) was increased in the model group compared to the control group ($P < 0.05$). OPD down-regulated the protein level of mTOR and p-mTOR compared to model group ($P < 0.01$). These results suggest that OPD treatment could reduce the translation level of mTOR in the liver. The protein level of SREBP1 and SCD1 was also significantly lower in the OPD group than that in the model group ($P < 0.01$). Additionally, the result of immunofluorescence staining showed that there was less positive staining of SREBP1 and SCD1 in OPD group compared with the model group (Fig. 5G). In a word, OPD improves lipid metabolism by inhibiting the mTOR/SREBP/SCD1 pathway.

*Oleate-Induced Lipid Accumulation Inhibited by OPD*

To investigate whether OPD could regulate lipid metabolism *in vitro*, $LO_2$ cells were incubated in the medium with oleate solution for 24 hrs. Intracellular lipids were then detected using ORO staining. $LO_2$ cells exposed to the oleate solution showed a clear increase in lipid droplets compared with the control (Fig. 6B). OPD inhibited lipid accumulation induced by oleate in $LO_2$ cells. These results were further confirmed by the quantification of intracellular TG content (Fig. 6C). Consistent with the results *in vivo*, OPD treatment inhibited the phosphorylation of mTOR (Fig. 6D). Taken together, these results suggest that the improvement of lipid metabolism by OPD might be involved in the regulation of the mTOR/SREBP1/SCD1 pathway.

*Composition of Gut Microbiota*

In the current study, 16S rDNA sequencing technology and multivariate analysis were employed to explore the effect of OPD on gut microbiota. Based on the OTU statistical results, the α-diversity of the samples was determined, and the Shannon index was displayed in Fig. 7A. After HFD feeding, the abundance of gut microbiota was decreased in the model group compared with that in the control group, but this negative impact was offset by OPD treatment.

Further, we analyzed the β-diversity to evaluate the overall structural changes of gut microbiota. Principal coordinate analysis (PCoA) scores based on unweighted UniFrac

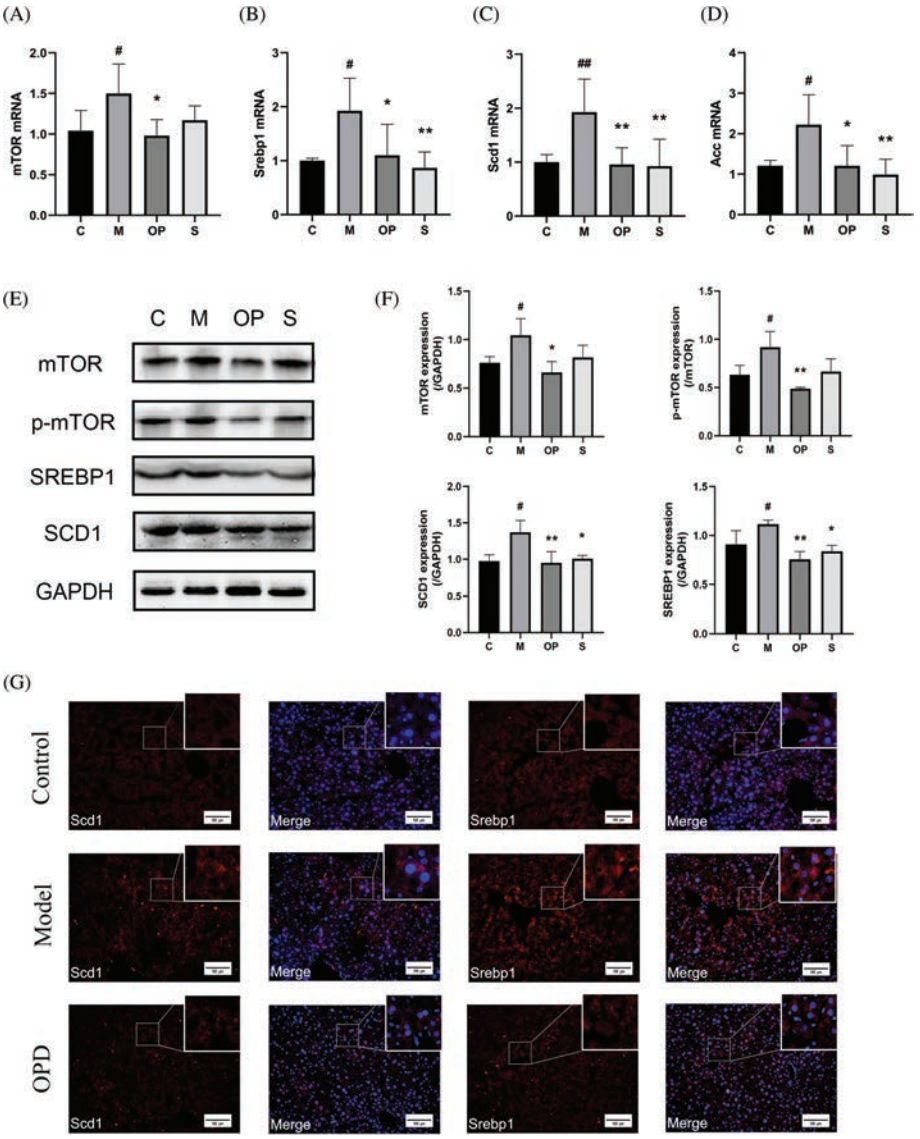


Figure 5. Ophiopogonin D changed the lipid metabolism related gene and protein level. (A–D) Relative mRNA levels of *mTOR*, *Srebp1*, *Scd1,* and *Acc* normalized with *Gapdh*. (E–F) Relative protein levels of mTOR, p-mTOR, SREBP1, and SCD1. (G) Immunofluorescence staining of SREBP1 and SCD1 in liver cryosection. Different superscript symbols indicate significant differences between groups ($^{\#}P < 0.05$ or $^{\#\#}P < 0.05$ vs. control group, $^{*}P < 0.05$ or $^{**}P < 0.01$ vs. model group).

analysis revealed that the model group was dissimilar from the control group. At the same time, PCoA based on weighted UniFrac analysis was consistent with the unweighted UniFrac PCoA analysis, indicating that OPD had a positive effect on the abundance and diversity of gut microbiota.

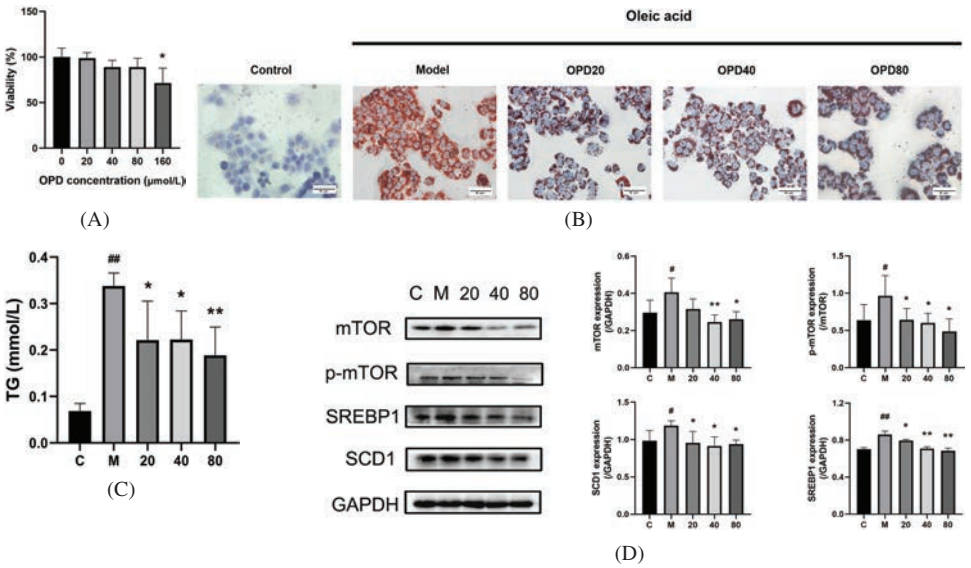


Figure 6. Inhibition of lipid accumulation in LO2 cells by OPD. (A) $LO_2$ cells were treated with the indicated concentrations of OPD for 24 hrs, and cytotoxicity was determined using the CCK8 assay. (B) $LO_2$ cells were treated with 300 μm/mL oleic acid for 24 hrs in the presence or absence of the indicated concentrations of OPD. Control cells did not treat with OPD. Cells were stained with Oil Red O. (C) Intracellular TG level was measured using a corresponding assay kit. (D) $LO_2$ cells were treated with various combinations of molecules as indicated, and then protein levels were determined. ($^{\#}P < 0.05$ or $^{\#\#}P < 0.05$ vs. control group, $^{*}P < 0.05$ or $^{**}P < 0.01$ vs. control group).

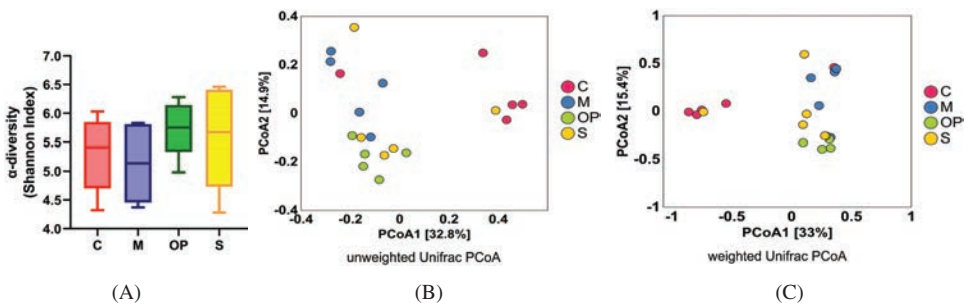


Figure 7. Ophiopogonin D changed the abundance and diversity of gut microbiota in $ApoE^{-/-}$ mice. (A) The Shannon index (an indicator of α-diversity in gut microbiota). (B) The unweighted UniFrac principal coordinate analysis (PCoA). (C) The weighted UniFrac PCoA. The PCoA evaluated the β-diversity of gut microbiota.

Taxon-based analysis was performed on OTUs to identify the changes in gut microbiota induced by a HFD (Fig. 8). Ten phyla were detected in all samples, which consisted of *Bacteroidetes* and *Firmicutes*. The relative abundance of *Firmicutes* was increased by a HFD, whereas the relative abundance of *Bacteroidetes* was noticeably diminished. Remarkably, the relative abundance of *Bacteroidetes* in the OPD group was increased from

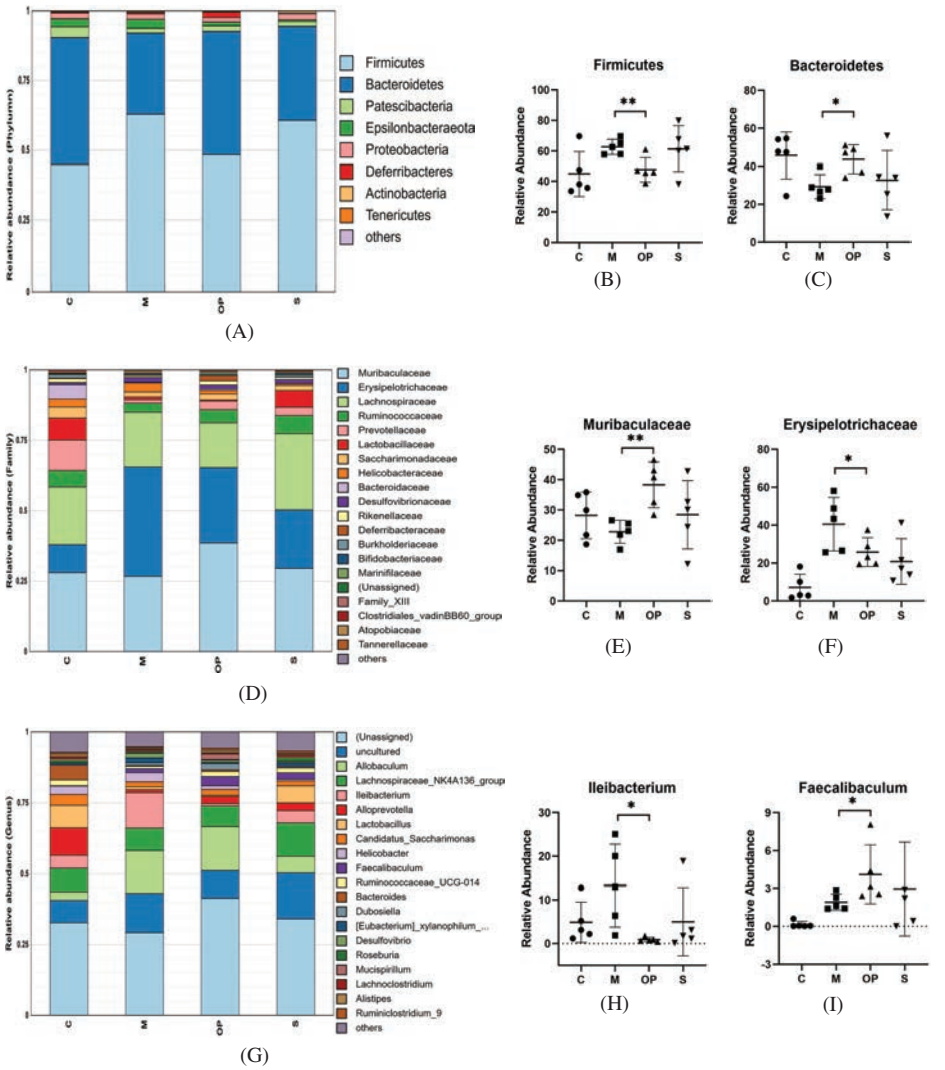


Figure 8. Ophiopogonin D changed the composition of gut microbiota in different levels. (A) The relative abundance of gut microbiota at the phylum level. (B–C) The relative abundance of the top 2 genera (*Firmicutes* and *Bacteroidetes*) at the phylum level. (D) The relative abundance of gut microbiota at the family level. (E–F) The relative abundance of the top 2 genera (*Muribaculaceae* and *Erysipelotrichaceae*) at the family level. (G) The relative abundance of gut microbiota at the genus level. (H–I) The relative abundance of significantly different 2 genera (*Ileibacterium* and *Faecalibaculum*) at the genus level. Different superscript symbols indicate significant differences between groups ($^{\#}P < 0.05$ or $^{\#\#}P < 0.05$ vs. control group, $^{*}P < 0.05$ or $^{**}P < 0.01$ vs. model group).

29.12% to 44.15% compared with that in the model group ($P < 0.05$), whereas the relative abundance of *Firmicutes* was decreased from 62.84% to 48.32% ($P < 0.05$). At the family level, the relative abundance of *Erysipelotrichaceae* was markedly decreased by OPD compared to the model group, whereas the relative abundance of *Muribaculaceae* was

markedly increased by OPD treatment. At the genus level, OPD had a significant enriching effect on the relative abundance of *Faecalibaculum* (from 1.40% to 3.25%, $P < 0.05$) and an inhibitory effect on the relative abundance of *Ileibacterium* (from 12.48% to 0.87%, $P < 0.05$) compared with those in the model group. Briefly, OPD remarkably changes the composition and the relative abundance of gut microbiota.

### *Fecal Metabolites of Mice*

As fecal metabolites are produced by gut microbiota, the content of fecal metabolites was examined to determine whether OPD also affected the fecal metabolites. 60 metabolites were detected by $^1$H NMR spectroscopy. The PLS-DA scores of the $^1$H NMR spectra for the four groups showed that the control (red) and model (green) groups had a different effect on the metabolic profile for fecal extracts. According to the PLS-DA, the variable importance in projection (VIP) scores were calculated, and potential metabolic biomarkers were identified (Fig. 9). Notably, leucine and acetate levels were persistently higher in the

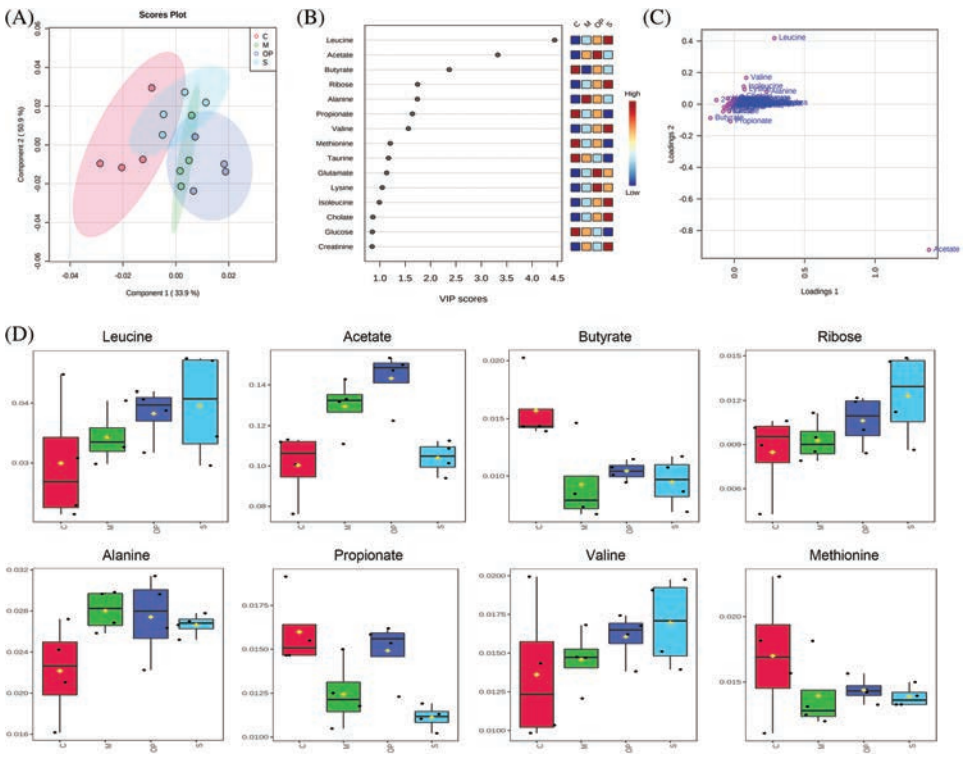


Figure 9. Ophiopogonin D changed the composition of fecal metabolites. (A) The PLS-DA Scores plots among the groups. (B) The variable importance in projection (VIP) scores were identified by PLS-DA. The colored boxes on the right indicate the relative concentrations of the corresponding metabolite in each group. (C) Loadings plot based on PLS-DA analysis. (D) The production of differential metabolites (leucine, acetate, butyrate, ribose, alanine, propionate, valine, and methionine).

OPD group than those in the model group. The butyrate level remained similar for that in the model and simvastatin groups. The levels of ribose, propionate, valine, methionine, glutamate, and lysine were all relatively higher in the OPD group compared to the model group. In a word, OPD changes the content of fecal metabolites.

## Discussion

The present study demonstrated that OPD treatment could slow plaque progression and possibly improve lipid metabolism by suppressing the mTOR/SREBP/SCD1 signaling pathway in ApoE$^{-/-}$ mice fed on a HFD. In addition, OPD improved hepatic steatosis and insulin resistance. Further studies showed that OPD changed the composition of gut microbiota as well as fecal metabolites. These findings illustrate that OPD could moderate lipid metabolism *in vivo* and *in vitro* as well as change the gut microbiota and metabolites in atherosclerotic mice.

CVDs, especially atherosclerosis, endanger the health of many people worldwide. Over past decades, studies have found that dysregulated lipid metabolism induces inflammation and immune response leading to atherosclerosis, and hyperglycemia is an independent risk factor for atherosclerosis (Tunon *et al.*, 2019). Lipid metabolism dysfunction, which is always caused by HFD, results in redundant lipid deposition in the organs, such as arteries and the liver (Xiong *et al.*, 2019). The transport of lipid to artery intimae, followed by deposition, leads to atherosclerotic lesion formation (Yu *et al.*, 2019).

In this study, we found that HFD resulted in a significant increase in the serum TG, TC, and LDL-C level, as well as a large plaque in aortic root. OPD treatment could moderate blood lipids mainly through decreasing the levels of TG, TC, and LDL-C instead of increasing the level of HDL-C. Further, OPD remarkably reduced the plaque size in the aortic root. HFD also induced a stress response with abnormal hepatic lipid accumulation, causing the loss of normal structure and function in the liver (Jing *et al.*, 2019), which contained various sizes of lipid droplets in the liver. In our study, we found that OPD treatment notably improved the function of the liver by lowering the levels of ALT and AST and alleviated macrovesicular steatosis of the liver induced by HFD.

In addition, some studies have demonstrated oxidative stress to be responsible for the simultaneous occurrence of insulin resistance, diabetes, and CVDs (Ceriello and Motz, 2004; Steven *et al.*, 2019). With the concentrations of free fatty acids, triglycerides, and cholesterol increased in HFD-fed mice, it results in an increased production of reactive oxygen species (ROS), which triggers oxidative stress (Vergani *et al.*, 2020; Li and Li, 2020). The antioxidant enzyme system responsible for eliminating ROS *in vivo* includes SOD, LDH, and MDA (Quan *et al.*, 2014). In the present study, we found that the level of MDA and LDH in the model group was significantly increased, while SOD decreased. After OPD treatment, the serum levels of MDA and LDH were decreased while SOD increased, demonstrating that OPD showed an anti-oxidative effect in mice.

Meanwhile, the level of ROS is closely related to insulin resistance and impaired function of pancreatic islet beta cells (Zhu *et al.*, 2019). As we know, the liver plays a pivotal role in maintaining blood glucose levels by balancing glucose storage and release

via glycogen synthesis and breakdown (Javary *et al.*, 2018). As the liver fatty injury was induced by the HFD, we found it caused insulin resistance in the model group. Fortunately, OPD improved glucose intolerance and insulin resistance in HFD-fed ApoE$^{-/-}$ mice.

It is known that mTOR is a member of the family of kinases associated with phosphatidylinositide 3-kinase and that it forms two distinct complexes: mTORC1 and mTORC2 (Mao and Zhang, 2018). Some studies have revealed that activation of mTOR promoted lipogenesis by activating the transcription of lipogenesis genes, including SREBP1, ACC, and SCD1 (Yin *et al.*, 2017; Xu *et al.*, 2016), while the inhibition of mTOR/SREBP1 signaling down-regulated expression of these lipogenic genes (Zhang *et al.*, 2018). mTORC1 regulates hepatic lipid metabolism through SREBP1, the main regulator of hepatic *de novo* lipogenesis (Luan *et al.*, 2020; Hao *et al.*, 2019). SREBP1 is initially synthesized as an inactive precursor and localized in the endoplasmic reticulum. In response to insulin signaling, SREBP1 is cleaved and transported to the nucleus to induce lipogenic gene expression. Liver-specific inhibition of mTORC1 abrogates SREBP1 function and renders mice resistant to hepatic steatosis and hypercholesterolemia induced by a Western diet (Mao and Zhang, 2018). As endothelial dysfunction occurs in the initial stage of atherosclerosis, the mTOR signaling pathway is involved in the endothelial injury induced by oxidative stress (Kurdi *et al.*, 2018). The use of the mTOR inhibitor, rapamycin, also reduces oxidative stress, modulates the inflammatory response and attenuates atherosclerotic progression in ApoE$^{-/-}$ mice (Pakala *et al.*, 2005). Furthermore, some research has indicated that mTOR plays a crucial role in glucose homeostasis: over-activation of mTOR in HFD-induced obese mice caused insulin resistance in the liver, with an mTOR inhibitor functioning as a glucose-lowering agent (Khamzina *et al.*, 2005; Korsheninnikova *et al.*, 2006). Therefore, inhibition of the mTOR/SREBP1/SCD1 pathway may have therapeutic potential for improving lipid metabolism, anti-oxidant, and glucose homeostasis.

In the present study, OPD treatment inhibited phosphorylation of mTOR and downstream SREBP1 and SCD1 in HFD fed ApoE$^{-/-}$ mice and $LO_2$ cells, indicating that OPD might improve lipid metabolism through suppressing the mTOR/SREBP1/SCD1 signaling pathway *in vivo* and *in vitro*. Numerous reports have found that the inhibitor of mTORC1 prevents the generation of foam cells, which induces atherosclerotic plaque formation and slows the progression of atherosclerosis in animal models (Martinet *et al.*, 2014). These findings provide the theoretical basis for exploring potential OPD effects to alleviate atherosclerosis.

The gut microbiome, a complex ecosystem of trillions of microorganisms, co-develops with the host and depends on the host genome, nutrition, and lifestyle (Nicholson *et al.*, 2012). Recently, there is increasing attention on the role of gut microbiota in CVDs like atherosclerosis: intestinal flora can improve atherosclerosis by regulating plasma lipid levels. It has been found that dysbiotic bacteria and their derived products trans-locating to the liver through a disrupted gut barrier, where they evoke a hepatic inflammatory reaction or metabolite interplays with dietary factors, resulting in lipid metabolism dysregultation in the liver (Kolodziejczyk *et al.*, 2019). Meanwhile, metabolic diseases induced by a HFD are characterized by loss of microbial diversity, particularly the ratio of *Bacteroidetes*/*Firmicutes*, which exerts multiple effects on host energy metabolism (Cao *et al.*, 2020).

Relative to lean mice and humans, obese individuals have an increased relative abundance of *Firmicutes* and a reduced abundance of *Bacteroidetes* (Hills *et al.*, 2019). Therefore, the gut microbiome plays an important role in metabolic diseases.

In the present study, the model group displayed a marked increase in body weight and a decreased ratio of *Bacteroidetes*/*Firmicutes* at the phylum level in gut microbiota. Our results showed that OPD not only significantly increased the relative abundance of *Bacteroidetes* but also decreased *Firmicutes* in HFD-fed ApoE$^{-/-}$ mice. Interestingly, OPD treatment resulted in distinctive microbiota composition at different classification levels: lower levels of *Erysipelotrichaceae* and higher levels of *Muribaculaceae* were observed in OPD group at the family level. A recent study has shown that *Muribaculaceae* taxa might have the effect of relieving HFD-induced obesity (Cao *et al.*, 2020). Several studies have confirmed an association between the *Erysipelotrichaceae* family and lipidemic profiles within the host. There was an increase of *Erysipelotrichaceae* in mice on a high-fat or Western diet (Fleissner *et al.*, 2010). The relative abundance of *Erysipelotrichi* was positively associated with changes in liver fat in female subjects who were placed on diets in which choline levels were manipulated (Spencer *et al.*, 2011). Furthermore, a correlation between the levels of *Erysipelotrichaceae* and host cholesterol metabolites has been identified (Martinez *et al.*, 2013). It suggested that the reduction of *Erysipelotrichaceae* might improve cholesterol homeostasis. In addition, researchers have found that excessive energy intake can lead to over-activation of mTORC1 signaling, resulting in homeostatic disruption and metabolic disorders. It has a direct effect on the composition of gut microbiota. The over-activation of the mTORC1 pathway would lead to suppression of the differentiation of intestinal goblet and Paneth cells. This suppression would lead to a reduction of mucus and antimicrobial peptides production and dysbiosis of gut microbiota (Noureldein and Eid, 2018; Zhou *et al.*, 2015).

In our study, there was a higher relative abundance of some beneficial bacteria in the OPD group, including *Faecalibaculum* and *Ruminococcaceae_UCG-014.* Recent studies have shown that *Faecalibaculum* could protect against intestinal tumor growth, and *Ruminococcaceae* and its genus *Ruminococcaceae_UCG-014* were reported to relieve HFD-induced obesity (Zagato *et al.*, 2020; Zhao *et al.*, 2017). Some other harmful genera were also found with lower abundance in the OPD group, including *Ileibacterium,* which belongs to the *Erysipelotrichaceae* family and is a new bacterial species isolated from the human ileum of a patient with Crohn disease (Mailhe *et al.*, 2017).

Additionally, the present study revealed that OPD increased the content of leucine and changed the metabolite composition. Leucine, a branched-chain amino acid, has been consistently correlated with the severity of insulin resistance as well as energy metabolism (Rivera *et al.*, 2020). Optimal dietary leucine levels significantly improve insulin signaling pathway-including targets of rapamycin and insulin receptor substrate 1, while high levels of leucine show an inhibitory effect (Liang *et al.*, 2019). Excessive dietary leucine could increase plasma triglyceride content by enhancing lipogenesis, through enhancing expression of SREBP1, ACC, and fatty acid syntheses. We also observed an obvious increase in the content of SCFAs in the OPD group, especially acetate, butyrate, and propionate. It has been demonstrated that SCFAs might increase fatty acid uptake and oxidation while preventing

lipid accumulation in skeletal muscle (Frampton *et al.*, 2020). Together, these findings indicate that the effect of OPD in improving lipid metabolism might partly depend on its modulation of gut microbiota and metabolites. However, how gut microbiota directly regulates lipid metabolism related gene expression remains unknown and should be further studied.

In conclusion, our results show that OPD regulates plasma lipid levels to slow down atherosclerosis progression in ApoE$^{-/-}$ mice. Additionally, OPD treatment could modulate gut microbiota and metabolites, providing a beneficial effect against insulin resistance and liver steatosis in HFD-fed ApoE$^{-/-}$ mice. This is the first time that the novel interaction between gut microbiota restoration and atherosclerosis improvement by OPD has been determined. This study indicates that OPD serves as a potential candidate for regulating gut microbiota to prevent atherosclerosis and metabolic diseases. However, further studies are necessary to elucidate the exact mechanism by which gut microbiota and lipid metabolism pathways are mutually regulated.



## Acknowledgments

This research was supported by grants from the National Natural Science Foundation of China (No. 81774213), Natural Science Foundation of Guangdong Province (No. 2018A030313436; No. 2018030310286), and the Hunan Provincial Science & Technology Department (No. 2018SK50501). Thanks to the technician from Magigen for excellent technical assistance.

## References

Alves, M.T., M.M.O. Ortiz, G.V.O.P. Dos Reis, L.M.S. Dusse, M.D.G. Carvalho, A.P. Fernandes and K.B. Gomes. The dual effect of C-peptide on cellular activation and atherosclerosis: Protective or not? *Diabetes Metab. Res. Rev*. 35: e3071, 2019.

Ardiansyah, Y. Inagawa, T. Koseki, A.Z. Agista, I. Ikeda, T. Goto, M. Komai and H. Shirakawa. Adenosine and adenosine-5'-monophosphate ingestion ameliorates abnormal glucose metabolism in mice fed a high-fat diet. *BMC Complement. Altern. Med*. 18: 304, 2018.

Cao, W., Y. Chin, X. Chen, Y. Mi, C. Xue, Y. Wang and Q. Tang. The role of gut microbiota in the resistance to obesity in mice fed a high fat diet. *Int. J. Food Sci. Nutr*. 71: 453–463, 2020.

Ceriello, A. and E. Motz. Is oxidative stress the pathogenic mechanism underlying insulin resistance, diabetes, and cardiovascular disease? The common soil hypothesis revisited. *Arterioscler. Thromb. Vasc. Biol*. 24: 816–823, 2004.

Chen, S., X. Li, L. Liu, C. Liu and X. Han. Ophiopogonin D alleviates high-fat diet-induced metabolic syndrome and changes the structure of gut microbiota in mice. *FASEB J*. 32: 1139–1153, 2018.

Fleissner, C.K., N. Huebel, M.M.A. El-Bary, G. Loh, S. Klaus and M. Blaut. Absence of intestinal microbiota does not protect mice from diet-induced obesity. *Br. J. Nutr*. 104: 919–929, 2010.

Frampton, J., K.G. Murphy, G. Frost and E.S. Chambers. Short-chain fatty acids as potential regulators of skeletal muscle metabolism and function. *Nat. Metab*. 2: 840–848, 2020.

Hao, T., H. Chen, S. Wu and H. Tian. LRG ameliorates steatohepatitis by activating the AMPK/mTOR/SREBP1 signaling pathway in C57BL/6J mice fed a highfat diet. *Mol. Med. Rep*. 20: 701–708, 2019.

Hills, R.D., B.A. Pontefract, H.R. Mishcon, C.A. Black, S.C. Sutton and C.R. Theberge. Gut microbiome: Profound implications for diet and disease. *Nutrients* 11: 1613, 2019.

Huang, Q., B. Gao, L. Wang, H.Y. Zhang, X.J. Li, J. Shi, Z. Wang, J.K. Zhang, L. Yang, Z.J. Luo and J. Liu. Ophiopogonin D: A new herbal agent against osteoporosis. *Bone* 74: 18–28, 2015.

Huang, X., Y. Wang, Z. Zhang, Y. Wang, X. Chen, Y. Wang and Y. Gao. Ophiopogonin D and EETs ameliorate Ang II-induced inflammatory responses via activating PPARalpha in HUVECs. *Biochem. Biophys. Res. Commun*. 490: 123–133, 2017.

Javary, J., N. Allain-Courtois, N. Saucisse, P. Costet, C. Heraud, F. Benhamed, R. Pierre, C. Bure, N. Pallares-Lupon, Cruzeiro M. Do, C. Postic, D. Cota, P. Dubus, J. Rosenbaum and S. Benhamouche-Trouillet. Liver Reptin/RUVBL2 controls glucose and lipid metabolism with opposite actions on mTORC1 and mTORC2 signalling. *Gut* 67: 2192–2203, 2018.

Jing, Y., Q. Sun, X. Xiong, R. Meng, S. Tang, S. Cao, Y. Bi and D. Zhu. Hepatocyte growth factor alleviates hepatic insulin resistance and lipid accumulation in high-fat diet-fed mice. *J. Diabetes Investig*. 10: 251–260, 2019.

Jonsson, A.L. and F. Backhed. Role of gut microbiota in atherosclerosis. *Nat. Rev. Cardiol*. 14: 79–87, 2017.

Khamzina, L., A. Veilleux, S. Bergeron and A. Marette. Increased activation of the mammalian target of rapamycin pathway in liver and skeletal muscle of obese rats: Possible involvement in obesity-linked insulin resistance. *Endocrinology* 146: 1473–1481, 2005.

Kolodziejczyk, A.A., D. Zheng, O. Shibolet and E. Elinav. The role of the microbiome in NAFLD and NASH. *EMBO Mol. Med*. 11: e9302, 2019.

Korsheninnikova, E., G.C. van der Zon, P.J. Voshol, G.M. Janssen, L.M. Havekes, A. Grefhorst, F. Kuipers, D.J. Reijngoud, J.A. Romijn, D.M. Ouwens and J.A. Maassen. Sustained activation of the mammalian target of rapamycin nutrient sensing pathway is associated with hepatic insulin resistance, but not with steatosis, in mice. *Diabetologia* 49: 3049–3057, 2006.

Kurdi, A., W. Martinet and G.R.Y. De Meyer. MTOR inhibition and cardiovascular diseases: Dyslipidemia and atherosclerosis. *Transplantation* 102: S44–S46, 2018.

Lacy, M., D. Atzler, R. Liu, M. de Winther, C. Weber and E. Lutgens. Interactions between dyslipidemia and the immune system and their relevance as putative therapeutic targets in atherosclerosis. *Pharmacol. Ther*. 193: 50–62, 2019.

Lee, J.H., C. Kim, S.G. Lee, G. Sethi and K.S. Ahn. Ophiopogonin D, a steroidal glycoside abrogates STAT3 signaling cascade and exhibits Anti-Cancer activity by causing GSH/GSSG imbalance in lung carcinoma. *Cancers* 10: 427, 2018.

Li, X. and X. Li. Obesity promotes experimental colitis by increasing oxidative stress and mitochondrial dysfunction in the colon. *Inflammation* 43: 1884–1892, 2020.

Liang, H., A. Mokrani, H. Chisomo-Kasiya, K. Ji, X. Ge, M. Ren, B. Liu, B. Xi and A. Sun. Dietary leucine affects glucose metabolism and lipogenesis involved in TOR/PI3K/Akt signaling pathway for juvenile blunt snout bream Megalobrama amblycephala. *Fish Physiol. Biochem*. 45: 719–732, 2019.

Luan, H., Z. Huo, Z. Zhao, S. Zhang, Y. Huang, Y. Shen, P. Wang, J. Xi, J. Liang and F. Wu. Scutellarin, a modulator of mTOR, attenuates hepatic insulin resistance by regulating hepatocyte lipid metabolism via SREBP-1c suppression. *Phytother. Res*. 34: 1455–1466, 2020.

Lv, Y., X. Gao, Y. Luo, W. Fan, T. Shen, C. Ding, M. Yao, S. Song and L. Yan. Apigenin ameliorates HFD-induced NAFLD through regulation of the XO/NLRP3 pathways. *J. Nutr. Biochem*. 71: 110–121, 2019.

Mailhe, M., D. Ricaboni, V. Vitton, J.C. Lagier, P.E. Fournier and D. Raoult. "*Ileibacterium massiliense*" gen. Nov., Sp. Nov., A new bacterial species isolated from human ileum of a patient with Crohn disease. *New Microbes New Infect*. 17: 25–26, 2017.

Mao, Z. and W. Zhang. Role of mTOR in glucose and lipid metabolism. *Int. J. Mol. Sci*. 19: 2043, 2018.

Martinet, W., H. De Loof and G.R.Y. De Meyer. MTOR inhibition: A promising strategy for stabilization of atherosclerotic plaques. *Atherosclerosis* 233: 601–607, 2014.

Martinez, I., D.J. Perdicaro, A.W. Brown, S. Hammons, T.J. Carden, T.P. Carr, K.M. Eskridge and J. Walter. Diet-induced alterations of host cholesterol metabolism are likely to affect the gut microbiota composition in hamsters. *Appl. Environ. Microbiol*. 79: 516–524, 2013.

Martin-Timon, I., C. Sevillano-Collantes, A. Segura-Galindo and F.J.D. Canizo-Gomez. Type 2 diabetes and cardiovascular disease: Have all risk factors the same strength? *World J. Diabetes* 5: 444–470, 2014.

Nagy, C. and E. Einwallner. Study of *in vivo* glucose metabolism in high-fat diet-fed mice using oral glucose tolerance test (OGTT) and insulin tolerance test (ITT). *J. Vis. Exp*. 131: 56672, 2018.

Nicholson, J.K., E. Holmes, J. Kinross, R. Burcelin, G. Gibson, W. Jia and S. Pettersson. Host-gut microbiota metabolic interactions. *Science* 336: 1262–1267, 2012.

Noureldein, M.H. and A.A. Eid. Gut microbiota and mTOR signaling: Insight on a new pathophysiological interaction. *Microb. Pathog*. 118: 98–104, 2018.

Ohira, H., W. Tsutsui and Y. Fujioka. Are short chain fatty acids in gut microbiota defensive players for inflammation and atherosclerosis? *J. Atheroscler. Thromb*. 24: 660–672, 2017.

Pakala, R., E. Stabile, G.J. Jang, L. Clavijo and R. Waksman. Rapamycin attenuates atherosclerotic plaque progression in apolipoprotein E knockout mice: Inhibitory effect on monocyte chemotaxis. *J. Cardiovasc. Pharmacol.* 46: 481–486, 2005.

Paoletti, R., C. Bolego, A. Poli and A. Cignarella. Metabolic syndrome, inflammation and atherosclerosis. *Vasc. Health Risk Manag*. 2: 145–152, 2006.

Park, J.E., M. Miller, J. Rhyne, Z. Wang and S.L. Hazen. Differential effect of short-term popular diets on TMAO and other cardio-metabolic risk markers. *Nutr. Metab. Cardiovasc. Dis*. 29: 513–517, 2019.

Quan, X., L. Zhang, Y. Li and C. Liang. TCF2 attenuates FFA-induced damage in islet beta-cells by regulating production of insulin and ROS. *Int. J. Mol. Sci*. 15: 13317–13332, 2014.

Rivera, M.E., E.S. Lyon, M.A. Johnson and R.A. Vaughan. Leucine increases mitochondrial metabolism and lipid content without altering insulin signaling in myotubes. *Biochimie* 168: 124–133, 2020.

Sang, S., X. Zhang, H. Dai, B.X. Hu, H. Ou and L. Sun. Diversity and predictive metabolic pathways of the prokaryotic microbial community along a groundwater salinity gradient of the Pearl River Delta, China. *Sci. Rep*. 8: 17317, 2018.

Simic, I. and Z. Reiner. Adverse effects of statins — myths and reality. *Curr. Pharm. Des*. 21: 1220–1226, 2015.

Sonnenburg, J.L. and F. Backhed. Diet-microbiota interactions as moderators of human metabolism. *Nature* 535: 56–64, 2016.

Spencer, M.D., T.J. Hamp, R.W. Reid, L.M. Fischer, S.H. Zeisel and A.A. Fodor. Association between composition of the human gastrointestinal microbiome and development of fatty liver with choline deficiency. *Gastroenterology* 140: 976–986, 2011.

Steven, S., K. Frenis, M. Oelze, S. Kalinovic, M. Kuntic, M.T. Bayo Jimenez, K. Vujacic-Mirski, J. Helmstadter, S. Kroller-Schon, T. Munzel and A. Daiber. Vascular inflammation and oxidative stress: Major triggers for cardiovascular disease. *Oxid. Med. Cell. Longev*. 2019: 7092151, 2019.

Tang, W.H., T. Kitai and S.L. Hazen. Gut microbiota in cardiovascular health and disease. *Circ. Res*. 120: 1183–1196, 2017.

Tunon, J., L. Badimon, M.L. Bochaton-Piallat, B. Cariou, M.J. Daemen, J. Egido, P.C. Evans, I.E. Hoefer, D.F.J. Ketelhuth, E. Lutgens, C.M. Matter, C. Monaco, S. Steffens, E. Stroes, C. Vindis, C. Weber and M. Back. Identifying the anti-inflammatory response to lipid lowering therapy: A position paper from the working group on atherosclerosis and vascular biology of the European Society of Cardiology. *Cardiovasc. Res*. 115: 10–19, 2019.

Vergani, L., F. Baldini, M. Khalil, A. Voci, P. Putignano and N. Miraglia. New perspectives of S-Adenosylmethionine (SAMe) applications to attenuate fatty Acid-Induced steatosis and oxidative stress in hepatic and endothelial cells. *Molecules* 25: 4237, 2020.

Wang, L., Y. Zhao, Q. Zhou, C.L. Luo, A.P. Deng, Z.C. Zhang and J.L. Zhang. Characterization and hepatoprotective activity of anthocyanins from purple sweet potato (*Ipomoea batatas* L. Cultivar *Eshu* No. 8). *J. Food Drug Anal*. 25: 607–618, 2017.

Wang, Y., X. Huang, Z. Ma, Y. Wang, X. Chen and Y. Gao. Ophiopogonin D alleviates cardiac hypertrophy in rat by upregulating CYP2J3 *in vitro* and suppressing inflammation *in vivo*. *Biochem. Biophys. Res. Commun*. 503: 1011–1019, 2018.

Xiong, Q., L. Zhu, F. Zhang, H. Li, J. Wu, J. Liang, J. Yuan, Y. Shi, Q. Zhang and Y. Hu. Protective activities of polysaccharides from Cipangopaludina chinensis against high-fat-diet-induced atherosclerosis via regulating gut microbiota in ApoE-deficient mice. *Food Funct*. 10: 6644–6654, 2019.

Xu, H.F., J. Luo, W.S. Zhao, Y.C. Yang, H.B. Tian, H.B. Shi and M. Bionaz. Overexpression of SREBP1 (sterol regulatory element binding protein 1) promotes de novo fatty acid synthesis and triacylglycerol accumulation in goat mammary epithelial cells. *J. Dairy Sci*. 99: 783–795, 2016.

Yin, F., G. Sharen, F. Yuan, Y. Peng, R. Chen, X. Zhou, H. Wei, B. Li, W. Jing and J. Zhao. TIP30 regulates lipid metabolism in hepatocellular carcinoma by regulating SREBP1 through the Akt/mTOR signaling pathway. *Oncogenesis* 6: e347, 2017.

Yu, X.H., D.W. Zhang, X.L. Zheng and C.K. Tang. Cholesterol transport system: An integrated cholesterol transport model involved in atherosclerosis. *Prog. Lipid Res*. 73: 65–91, 2019.

Zagato, E., C. Pozzi, A. Bertocchi, T. Schioppa, F. Saccheri, S. Guglietta, B. Fosso, L. Melocchi, G. Nizzoli, J. Troisi, M. Marzano, B. Oresta, I. Spadoni, K. Atarashi, S. Carloni, S. Arioli, G. Fornasa, F. Asnicar, N. Segata, S. Guglielmetti, K. Honda, G. Pesole, W. Vermi, G. Penna and M. Rescigno. Endogenous murine microbiota member Faecalibaculum rodentium and its human homologue protect from intestinal tumour growth. *Nat. Microbiol*. 5: 511–524, 2020.

Zhang, T., F. Huang, B. Li, C. Huang, C. Xu, K. Lin and D. Lin. NMR-based metabolomic analysis for the effects of Huiyang Shengji extract on rat diabetic skin ulcers. *J. Ethnopharmacol*. 261: 112978, 2020.

Zhang, T., J. Huang, Y. Yi, X. Zhang, J.J. Loor, Y. Cao, H. Shi and J. Luo. Akt Serine/Threonine Kinase 1 Regulates *de Novo* Fatty Acid Synthesis through the Mammalian Target of Rapamycin/Sterol Regulatory Element Binding Protein 1 Axis in Dairy Goat Mammary Epithelial Cells. *J. Agric. Food Chem*. 66: 1197–1205, 2018.

Zhao, L., Q. Zhang, W. Ma, F. Tian, H. Shen and M. Zhou. A combination of quercetin and resveratrol reduces obesity in high-fat diet-fed rats by modulation of gut microbiota. *Food Funct*. 8: 4644–4656, 2017.

Zhou, Y., P. Rychahou, Q. Wang, H.L. Weiss and B.M. Evers. TSC2/mTORC1 signaling controls Paneth and goblet cell differentiation in the intestinal epithelium. *Cell Death Dis*. 6: e1631, 2015.

Zhu, X.A., L.F. Gao, Z.G. Zhang and D.K. Xiang. Down-regulation of miR-320 exerts protective effects on myocardial I-R injury via facilitating Nrf2 expression. *Eur. Rev. Med. Pharmacol. Sci*. 23: 1730–1741, 2019.